ACS Catalysis

pubs.acs.org/acscatalysis
Research Article

Realistic Fuel Cell Catalyst Degradation via Automated Identical Location SEM-PSD Analysis with the GDE Half-Cell Setup

Mitja Kostelec,* Goran Dražić, Ana Rebeka Kamšek, Jan Vidergar, Gregor Kapun, and Nejc Hodnik*

Cite This: ACS Catal. 2026, 16, 11207−11218
Read Online

ABSTRACT: A realistic evaluation of electrocatalyst stability requires experimental setups that accurately reproduce the coupled chemical and transport environments of membrane-electrode assemblies. Conventional GDE half-cells, however, are typically operated without a proton-exchange membrane, exposing the catalyst layer directly to liquid electrolytes and intensifying dissolution-migration-redeposition dynamics. Here, we examine how the presence of a membrane alters degradation in PtCo/C catalyst layers and establish a quantitative workflow for tracking nanoparticle evolution under realistic conditions. Particle-size distributions (PSDs) are extracted directly from low-kV identical-location SEM (IL-SEM) images of intact, micrometer-thick porous catalyst layers and validated against IL-TEM for surface-accessible particles. Automated segmentation enables robust, high-throughput analysis across large datasets. Applying this framework to accelerated stress tests reveals that membrane-free GDEs undergo pronounced coarsening driven by severe Pt dissolution and redeposition under direct acid exposure, whereas membrane-protected electrodes constrain transport pathways and therefore exhibit more moderate, representative degradation behaviour. These findings underscore the indispensable role of the membrane for realistic half-cell durability studies and demonstrate that automated IL-SEM-based PSD analysis provides a powerful framework for linking morphological evolution to electrochemical performance in complex, three-dimensional porous electrocatalyst systems.

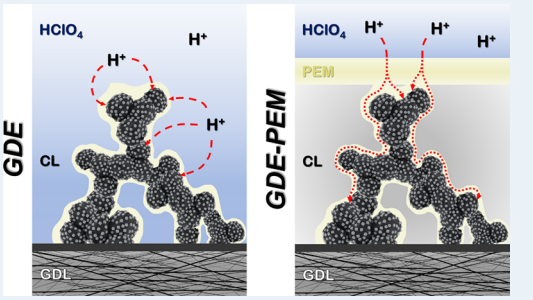

KEYWORDS: *proton-exchange membrane fuel cell (PEM FC), particle-size distribution (PSD), identical-location scanning electron microscopy (IL-SEM), gas diffusion electrode half-cell setup (GDE), nanoparticles*

1. INTRODUCTION

Proton-exchange membrane fuel cells (PEM FCs) are among the most promising clean energy conversion technologies due to their high power density, low operating temperature, and zero-emission operation.[1−3] Their long-term performance depends critically on the structural stability of the cathode catalyst layer, where Pt or Pt-based alloy nanoparticles are dispersed within a porous carbon-ionomer network that mediates electron, proton, and gas transport. Even small changes in particle-size distribution (PSD) or spatial arrangement can significantly influence catalytic activity and durability, highlighting the importance of understanding how these nanostructures evolve under operating conditions.[4−6]

The gas diffusion electrode (GDE) half-cell setup has become an increasingly valuable platform for bridging the gap between idealised model electrodes and the realistic environment of membrane-electrode assemblies (MEAs).[7−10] GDEs provide a representative porous catalyst architecture, improved gas accessibility, and compatibility with advanced ex-situ and in-situ imaging approaches. However, in most GDE studies the proton-exchange membrane is intentionally omitted for simplicity, leaving the catalyst layer fully exposed to liquid electrolyte. This modification alters local chemical gradients and removes transport constraints inherent to MEAs, often amplifying dissolution, migration, and Ostwald ripening processes.[8−12] As a result, degradation observed in membrane-free half-cells may significantly overestimate the severity and nature of catalyst evolution under realistic PEM FC conditions.

Characterising catalyst degradation therefore requires direct visualisation within intact, micrometer-thick porous catalyst layers, where transport pathways and the local environment resemble those in operating fuel cells. Although transmission electron microscopy (TEM) provides sub-nanometer resolution, it is limited to ultrathin samples and cannot capture the hierarchical morphology, depth gradients, and through-thickness transport present in practical catalyst layers.[4,5,13] Scanning electron microscopy (SEM), when operated under optimised low-kV conditions, can resolve Pt nanoparticles

Received: February 18, 2026
Revised: April 14, 2026
Accepted: April 30, 2026
Published: May 14, 2026

https://doi.org/10.1021/acscatal.6c01369
ACS Catal. 2026, 16, 11207−11218

directly on intact electrodes and preserve their native structural context.[13−16] This capability enables PSD analysis of surface-accessible nanoparticles on intact, micrometer-thick catalyst layers, providing information from realistic electrode architectures that are inaccessible to conventional TEM.

To exploit this advantage, we establish an SEM-based methodology for extracting statistically meaningful PSDs directly from intact catalyst layers. The approach is validated by identical-location TEM (IL-TEM) and combined with automated segmentation to enable unbiased, high-throughput analysis.[14,15,17−21] Using this framework, we compare GDE half-cells with and without a proton-exchange membrane under identical accelerated stress testing (AST) protocols. This study demonstrates that membrane inclusion is essential for realistic catalyst stability evaluation and establishes IL-SEM-based PSD analysis as a robust tool for nanostructural characterisation under conditions relevant to PEM fuel cell operation.[7−10,22,23]

2. EXPERIMENTAL SECTION

Materials

The PtCo/C electrocatalyst used in this study was supplied by ReCatalyst d.o.o. (Slovenia). This catalyst was selected as a technologically relevant, state-of-the-art PEMFC cathode material and because its physicochemical and electrochemical characteristics had previously been benchmarked against commercial PtCo/C catalysts from Umicore (Elyst Pt30 0690 and Elyst Pt50 0690), including MEA-level evaluation. In addition, its nanoparticle size distribution had previously been characterised by TEM, making it a suitable reference material for the present SEM/PSD methodology study.[24] Catalyst layers for IL-SEM studies were prepared by spray-coating, which ensures uniform deposition and well-controlled loading across the gas diffusion layer (GDL).[25] A platinum loading of approximately 0.5 mgPt cm^{-2} was applied, representative of cathode catalyst layers in MEAs.

For experiments involving a proton-exchange membrane, a membrane[26] was laminated onto the GDE by hot-pressing. This yielded stable interfacial contact and low resistance while preserving the native catalyst layer morphology.

Details of the materials and preparation steps are provided in the Supporting Information.

Scanning Electron Microscopy

SEM imaging was conducted using a Thermo Fisher Apreo 2S field-emission scanning electron microscope operated at an accelerating voltage of 2 kV in high vacuum. The low accelerating voltage increases surface sensitivity and restricts the electron interaction volume within the carbon matrix, thereby enhancing nanoparticle contrast. A low beam current (∼13 pA) was used to minimise beam-induced carbon deposition and surface charging while maintaining a small, stable probe suitable for high-resolution SEM imaging. Secondary electron (SE) and backscattered electron (BSE) detectors were used simultaneously to provide complementary topographical and compositional contrast.[27−29]

Under the ultra-low-kV imaging conditions used here, detector contrast in the Trinity system depends on both electron energy and trajectory within the column field. At such low landing energies, the electron interaction volume is strongly reduced, rendering even the BSE-enriched T1 signal highly surface sensitive and enabling sufficiently high spatial resolution for reliable nanoparticle identification and segmentation. For quantitative particle segmentation and PSD analysis, the T1 detector was therefore used, since it preferentially collects higher-energy BSE and provided the strongest and most reproducible material-sensitive contrast between PtCo nanoparticles and the carbon support. For representative IL-SEM figures, a T1 + T3 overlay was used for visualisation, combining strong nanoparticle contrast from T1 with enhanced rendering of carbon edges and surface features from the low-energy SE signal collected by T3.[27−29]

Before imaging, the samples were thoroughly rinsed with Milli-Q water. Hydrocarbon contamination was minimised primarily through careful SEM operating conditions, including avoidance of ethanol washing, high-vacuum imaging, and low-dose acquisition parameters selected to reduce beam-induced carbon deposition. No conductive coating was applied to preserve the native catalyst layer (CL) structure, enabling true surface characterisation and avoiding interference with electrochemical measurements during IL experiments. Chamber pressure during imaging was maintained below 1×10^{-4} Pa.

Identical-location SEM (IL-SEM) was performed by registering distinctive morphological features, such as scratches, pore geometries, or carbon agglomerates, as fiducial markers. This enabled relocation of the same regions before and after electrochemical treatment, following established protocols.[21,30]

Transmission Electron Microscopy

Scanning transmission electron microscopy (STEM) was performed using a JEOL ARM 200 CF microscope equipped with a cold field-emission gun and a probe Cs corrector. Catalyst powder was transferred onto an Au holey carbon TEM grid and imaged at 80 kV to minimise electron-beam damage. High-angle annular dark-field (HAADF) imaging was used to maximise Z-contrast between PtCo nanoparticles and the carbon support. Details of the imaging conditions and pre-processing steps are provided in the Supporting Information.

Image Processing

SEM images were processed using ImageJ (NIH, USA) to enhance clarity and enable reproducible particle segmentation. All images within a dataset were processed using identical parameters, including Gaussian or median filtering, background correction, and morphological opening or closing to suppress noise and improve particle boundary definition.

Automated segmentation was implemented to minimise operator bias and enable high-throughput particle size extraction. The workflow employed adaptive thresholding to identify nanoparticle features, followed by a distance-transform watershed algorithm to separate touching particles. Additional shape- and spacing-based criteria were applied to avoid artificial splitting or merging of particles. Objects intersecting image borders were excluded from analysis.

Particle areas were converted to equivalent circular diameters and used to construct PSD histograms, violin plots, and box-and-whisker summaries. Thresholds for minimum and maximum particle size ensured exclusion of artefacts. Segmentation performance was validated against IL-TEM and manually segmented datasets.

The full segmentation workflow, including all processing steps and parameter choices, is described in detail in the Supporting Information, ensuring reproducibility using standard open-source image-processing tools.

Electrode Preparation, Cell Assembly, and Electrochemical Measurements

Electrochemical measurements were conducted in (i) a standard GDE half-cell configuration[31] (Figure 1a) and (ii) a modified floating electrode (MFE) configuration for thin-film TEM grid samples (Figure 1b).[16] In the GDE setup, the catalyst-coated GDL served as the working electrode, with the catalyst layer facing the electrolyte. A reversible hydrogen electrode (HydroFlex, Gaskatel) was used as the reference electrode, and an IrTa-coated titanium mesh served as the counter electrode. In the MFE setup, a TEM grid with drop-cast catalyst acted as the working electrode.

All measurements were performed at room temperature using a BioLogic SP-200 potentiostat with EC-Lab software. The electrolyte was 2 M $HClO_4$ for all experiments except in the study of electrolyte effect, where 0.5 M and 0.1 M $HClO_4$ were also used.

https://doi.org/10.1021/acscatal.6c01369
ACS Catal. 2026, 16, 11207−11218

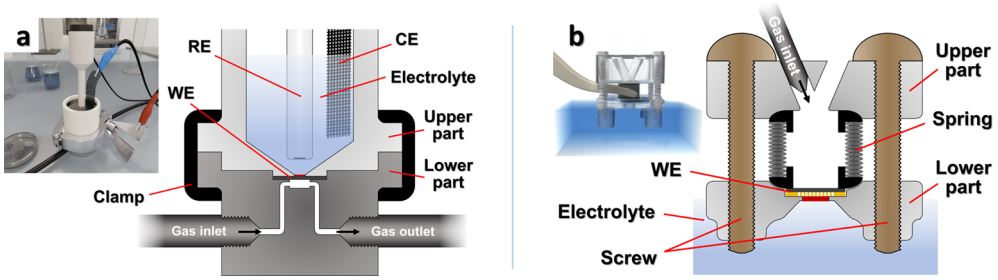

Figure 1. Schematic comparison of (a) GDE and (b) MFE setup configurations. The sample serves as the working electrode (WE), a reversible hydrogen electrode (RHE, HydroFlex) is used as the reference electrode (RE), and an IrTa-coated titanium mesh functions as the counter electrode (CE). The 3D schematic of the MFE (part of b) is adapted from ref 16, distributed under a Creative Commons Attribution License (CC BY).

The primary accelerated stress test (Protocol 1), adapted from the U.S. DOE AST procedure,[7] consisted of 30 000 potential steps between 0.60 and 0.95 V (3 s holds at each potential) under nitrogen. The severe dissolution protocol (Protocol 2) used the same cycling in oxygen-saturated electrolyte, resulting in severe Pt dissolution in our flooded, membrane-free GDE.[32,33] Protocol 2 was used only as a deliberately severe stress condition to visualise the effect of beam-induced carbon contamination in IL-SEM, and not for the membrane-effect study. The severe ripening protocol (Protocol 3) consisted of 2000 scans between 0.05 and 1.60 V at 500 mV s^{-1} under nitrogen. Protocol 3 was used to enhance the contrast between samples and thereby make the effect of acid exposure more visually apparent.

Additional procedural details, including conditioning steps and cell geometries, are provided in the Supporting Information.

3. RESULTS AND DISCUSSION

To evaluate how the proton-exchange membrane influences degradation pathways in realistic catalyst layers, we first established an SEM-based PSD methodology capable of quantifying nanoparticle evolution directly within intact, micrometer-thick porous GDE catalyst layers. Conventional TEM, although offering sub-nanometer resolution, is inherently limited to ultrathin specimens and cannot capture the hierarchical architecture or interlayer transport present in practical electrodes, making it unsuitable for studying degradation in real GDE catalyst layers.

Architectural Effects—2D versus 3D Ripening in MFE and GDE Catalyst Layers

To isolate the influence of catalyst-layer architecture on degradation, we compared two systems subjected to the same severe ripening protocol (Protocol 3): (i) a thin-film PtCo/C catalyst on a TEM grid evaluated in the modified floating electrode (MFE) setup, representing a quasi-two-dimensional (2D) system, and (ii) a micrometer-thick PtCo/C catalyst layer in a GDE configuration, representing a fully three-dimensional (3D) porous architecture.

IL-SEM images recorded before and after cycling reveal striking differences between the two systems (Figure 2). In the MFE thin film, coarsening is modest. This behaviour is characteristic of lateral 2D Ostwald ripening, in which dissolved Pt species migrate over short in-plane distances and redeposit locally.[9] The minimal film thickness effectively confines dissolution-migration-redeposition dynamics to a quasi-two-dimensional plane.

In the GDE, smaller particles dissolve and the resulting Pt species migrate over longer distances before redepositing onto larger particles located at different depth levels within the

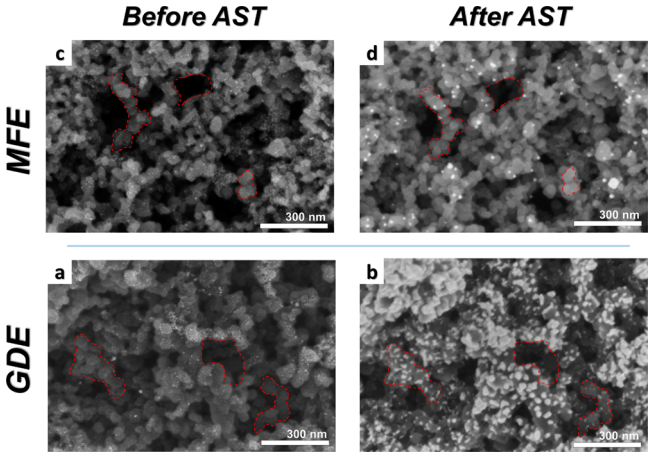

Figure 2. Comparison of PtCo/C catalyst coarsening in MFE and GDE setups after AST (Protocol 3). IL-SEM comparison: (a,c) before and (b,d) after AST. Large PtCo agglomerates are much more numerous and vary in size across different depth levels within the GDE catalyst layer, illustrating enhanced "3D" ripening compared to the "2D" ripening observed in the MFE. Red dashed contours mark identical fields of view to aid direct spatial correlation.

porous catalyst layer. This extended transport path enables vertically coupled coarsening, resulting in a characteristic shift in PSD towards significantly larger diameters.

Comparison of the GDE and MFE samples shows that catalyst-layer thickness and morphology fundamentally determine the dominant degradation mechanism. In thin-film MFE samples, Pt dissolution and redeposition occur predominantly laterally within a single layer, giving rise to 2D Ostwald ripening. In contrast, micrometer-thick porous GDE catalyst layers allow dissolved Pt species to migrate through the catalyst-layer thickness, enabling 3D ripening across different depth levels that produces far more pronounced particle coarsening.

These observations demonstrate that thin-film model systems systematically underrepresent degradation severity by suppressing interlayer transport pathways.[5] Realistic evaluation of electrocatalyst stability therefore requires catalyst-layer architectures that preserve the vertical ion-transport environment characteristic of PEM FC operation.

Nanoparticle Size Distribution Obtained with SEM

To quantitatively track nanoparticle evolution in micrometer-thick porous catalyst layers, we developed a PSD analysis

https://doi.org/10.1021/acscatal.6c01369
ACS Catal. 2026, 16, 11207−11218

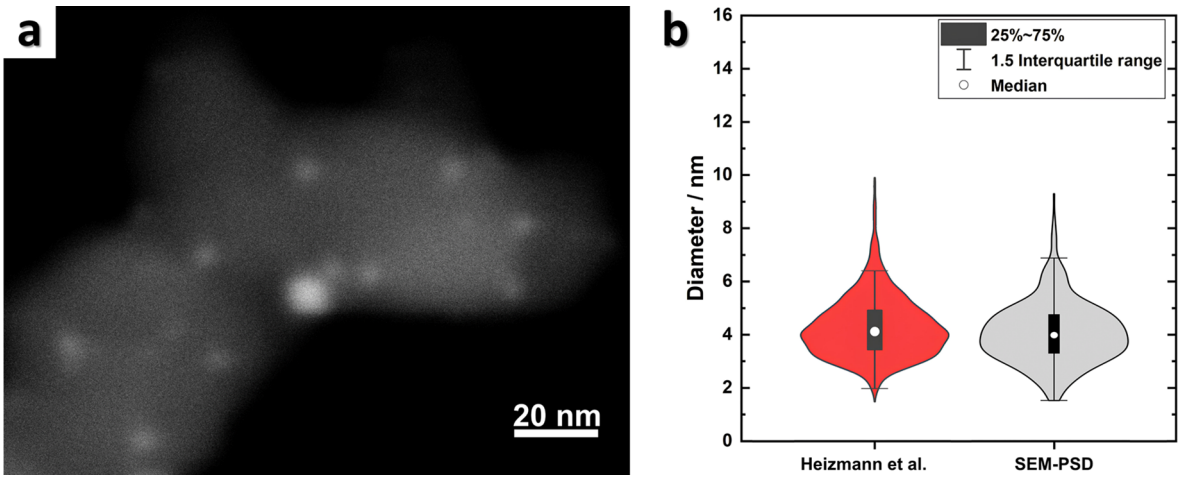

Figure 3. SEM characterisation of the catalyst. (a) Representative high-resolution SEM micrograph of Pt nanoparticles supported on carbon (bright spots). (b) Violin plot of the PSD reported in the literature[24]compared with that obtained from SEM analysis. The median diameter is approximately 4 nm, consistent with the nominal catalyst specification.

workflow based on SEM. Low-kV (1–2 kV) imaging provides a nominal surface-sensitive resolution of approximately 1–2 nm, which is sufficient to identify Pt nanoparticles of 2 nm or larger as distinct bright features against the carbon matrix and enables sampling across representative electrode areas without invasive thinning.

In SEM images (Figure 3a), the carbon support appears as a dark matrix, while Pt nanoparticles (approximately 2–5 nm in diameter, occasionally larger) appear as bright, roughly circular spots due to Z-contrast. To ensure reproducibility, at least five distinct regions were examined; all showed uniform Pt dispersion across the carbon support, and no charging effects were observed.

The resulting particle size distribution (Figure 3b) is approximately log normal, with a median diameter near 4 nm, closely matching the nominal catalyst specification and consistent with prior TEM reports.[24] The distribution shows a minor tail towards larger sizes (approximately 8–10 nm), indicating occasional agglomerates, and yields an average particle diameter of approximately 4 nm.

The SEM analysis revealed several key advantages for characterising platinum nanoparticles in PEM fuel-cell catalyst layers. First, although SEM generally offers lower ultimate resolution than TEM,[34] the ultra-high-resolution field-emission SEM (UHR-FEG-SEM) used in this study clearly resolved individual platinum nanoparticles with diameters of approximately 4 nm and, in some cases, distinguished features down to about 2 nm under low-voltage imaging conditions. Second, UHR-SEM enables direct imaging of the intact GDE surface without the need for laborious sample thinning or transfer to a TEM grid. As a result, particles are examined in their native electrode environment, providing a realistic assessment of their size and spatial distribution. Third, UHR-SEM imaging under the selected conditions proved non-destructive: identical electrode regions could be subjected to electrochemical testing without measurable changes in performance, confirming that the imaging process did not alter the structural integrity or electrochemical behaviour of the catalyst layer.

Unlike TEM, which records signals transmitted through the entire specimen thickness, UHR-SEM is inherently surface-sensitive. In TEM, even under ideal conditions, particles from multiple depth levels overlap in the projection image, causing distinct particles to appear merged and complicating both counting and size determination.[20] Although tilt-series imaging (tomography) and post-processing can mitigate these artefacts, they greatly increase dataset acquisition time. UHR-SEM avoids this limitation, enabling high-throughput imaging in which each field of view contains hundreds of well-separated, easily countable nanoparticles. As a result, thousands of particles can be analysed per sample, yielding statistically robust PSDs that often exceed the throughput achievable with TEM-based analyses. This surface sensitivity is particularly advantageous for industrially relevant catalysts with higher Pt loadings, where overlapping is even more pronounced in TEM, making it difficult to distinguish between agglomeration, coalescence, or mere projection overlap. By avoiding these ambiguities, UHR-SEM provides more reliable characterisation of particle size and distribution under realistic electrode conditions. The reported PSDs therefore represent the SEM-visible near-surface nanoparticle population, while possible depth-dependent differences in degradation are not directly resolved.

Validation of SEM-Derived PSDs by TEM

To verify the accuracy of SEM-based PSD measurements, an identical-location SEM/TEM workflow was developed to enable a one-to-one comparison of individual nanoparticles imaged by both techniques. A catalyst region was first imaged by SEM and subsequently relocated in the TEM using fiducial surface features such as scratches, carbon grain patterns, or agglomerates (Figure 4a,b). A high-angle annular dark-field STEM (HAADF-STEM) image was then acquired at 0° tilt to closely approximate the SEM viewing geometry.

To distinguish particles belonging to the SEM-visible surface from particles located deeper within the TEM projection, a limited IL-TEM tilt-series analysis was performed on the same catalyst region (see Supporting Information). Imaging the region at several tilt angles improved spatial orientation relative to the carbon support and enabled assignment of particles to the front-side surface, the back side of the carbon support, or intermediate depth. Only particles confidently assigned to the

https://doi.org/10.1021/acscatal.6c01369
ACS Catal. 2026, 16, 11207−11218

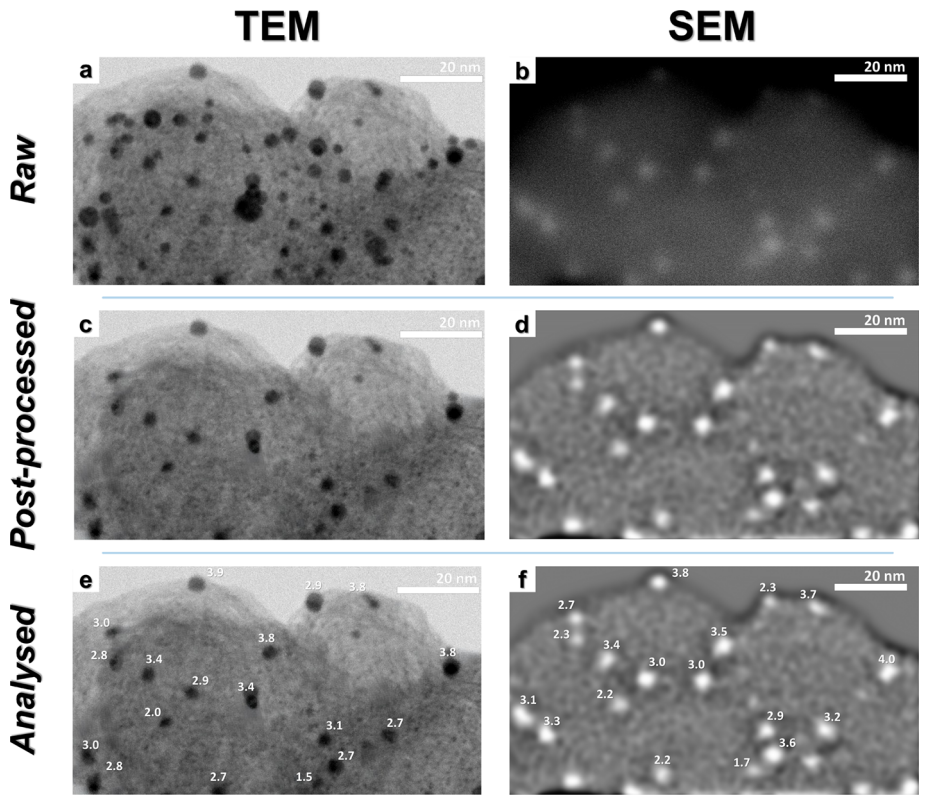

Figure 4. Validation of SEM sizing by TEM. The same catalyst region imaged by TEM (HAADF-STEM) at zero tilt (left column) and by UHR-SEM (right column). (a) Raw TEM image. (b) Raw SEM image. (c) Processed TEM image with bottom-layer particles removed. (d) Processed SEM image with enhanced particle resolution. (e, f) Analyzed processed images from TEM (e) and SEM (f).

front-side surface were retained, whereas particles not unambiguously belonging to this SEM-visible population were digitally removed from the processed TEM image. This step was introduced solely to enable an unambiguous one-to-one comparison of the very same particles imaged by TEM and SEM, and to calibrate the SEM-based sizing/segmentation workflow. In particular, the matched TEM-SEM comparison was used to define the effective particle-edge criterion applied in SEM images and to establish the practical lower size limit at which particle boundaries can still be reliably identified and measured by SEM under the applied imaging conditions. Accordingly, the TEM images in Figure 4 were not used for independent PSD determination. Particle diameters were then measured for the matched particles in the corresponding SEM and TEM images (Figure 4c,d).

This IL-SEM/TEM workflow provides robust validation of the SEM-based PSD method. By focusing exclusively on particles accessible to both techniques, it eliminates geometric artefacts arising from the depth-integrating nature of TEM. The results confirm that SEM can reliably and accurately characterise the PSD of SEM-visible surface/near-surface platinum nanoparticle population in PEM FC catalyst layers, even in complex, realistic environments such as GDE half-cells. Because IL-SEM in top-view geometry is inherently surface-sensitive, these PSDs should be interpreted as near-surface PSDs rather than full through-thickness distributions. It is worth noting that degradation within the catalyst layer is not necessarily uniform; literature reports indicate that the membrane-adjacent (near-surface) region often exhibits more pronounced Pt depletion, while deeper regions of the catalyst layer can be comparatively less affected depending on local transport conditions and operating regime.[35] Additionally, top-view IL-SEM could be complemented by FIB-based cross-sectional analysis to assess whether the degradation trends observed for the near-surface population are consistent across different depths of the catalyst layer, thereby improving confidence in the broader representativeness of the observed PSD evolution.

The analysed images (Figure 4e,f) show that particle diameters from SEM and TEM overlap almost completely, with only minor deviations attributable to operator bias. After excluding subsurface particles from the TEM dataset, both methods yield statistically comparable PSDs.

By validating SEM with IL-TEM, we establish confidence in using SEM alone for PSD measurements. This eliminates concerns that SEM might systematically under- or overestimate particle sizes due to contrast or resolution limitations. In practice, SEM imaging can be performed before and after electrochemical testing at identical locations, with full confidence that the PSDs obtained are reliable.

Postprocessing Automation

Quantitative analysis of nanoparticle degradation in realistic catalyst layers requires the evaluation of thousands of particles across multiple identical-location SEM images. Manual particle identification is time-consuming and inherently susceptible to operator bias, particularly when comparing PSDs across different degradation states.[20] To enable statistically meaningful

https://doi.org/10.1021/acscatal.6c01369
ACS Catal. 2026, 16, 11207−11218

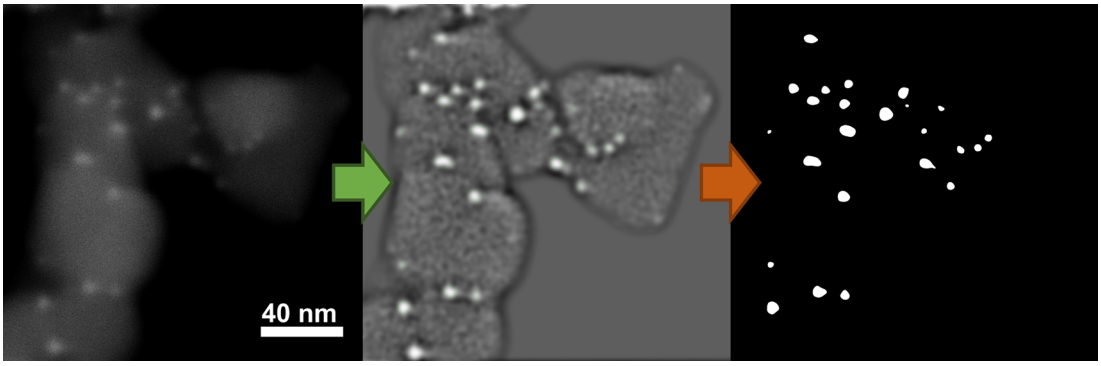

Figure 5. Representative example of micrograph analysis with automated nanoparticle segmentation from a high-resolution SEM image of a PtCo/C catalyst layer. Bright features correspond to Pt nanoparticles. The overlay shows the corresponding segmentation mask used for PSD analysis. The first step illustrates initial manual image pre-processing, while the second step presents automated segmentation.

and reproducible analysis, an automated segmentation pipeline was therefore employed.[36,37]

Figure 5 shows a representative example of automated nanoparticle segmentation from a high-resolution SEM micrograph. The automated approach reliably identifies individual Pt nanoparticles and produces consistent particle masks across large datasets. A typical SEM image was processed within seconds, enabling high-throughput analysis of thousands of nanoparticles per sample and allowing PSDs to be constructed with strong statistical confidence.

The automated results were benchmarked against manually segmented datasets and showed excellent agreement in all relevant PSD metrics. Minor discrepancies were limited to particles near the practical SEM detection limit or closely spaced particles and had no measurable influence on the resulting PSD trends. Importantly, all qualitative degradation trends reported in this work were reproduced using manually segmented subsets, confirming that the automated analysis does not influence the scientific conclusions.

Challenges of IL-SEM in Electrochemical Studies

Although SEM is generally considered less damaging to specimens than TEM,[38,39] it remains susceptible to electron-beam-induced carbon contamination. This effect may arise predominantly from dissociation and polymerisation of adsorbed hydrocarbon species introduced during sample handling or from the microscope environment; however, in carbon-supported catalyst layers, contributions from carbonaceous components intrinsic to the specimen cannot be fully excluded. In the present work, the likelihood of exogenous contamination was reduced by keeping the samples under high vacuum overnight before SEM analysis, which promotes desorption of part of the weakly adsorbed species from both the specimen surface and its immediate surroundings, including the holder/stage region. In addition, the SEM chamber was routinely cleaned using the integrated plasma cleaner and was cleaned prior to measurement. These precautions reduce the likelihood of contamination arising from the chamber and the direct vicinity of the specimen. Nevertheless, because specimen-derived carbonaceous contributions may still occur under electron-beam exposure, mitigation of this artefact depends not only on limiting external contamination, but equally on careful beam management, including low-dose imaging, short dwell times, stable high-vacuum conditions, and avoidance of repeated exposure of identical locations before electrochemical testing. While this process is well documented in TEM/STEM for its impact on imaging and analysis quality,[12,17,38,40] its implications for operando or durability-linked SEM studies are often underestimated. In IL-SEM, where the same region is repeatedly imaged before and after electrochemical testing, progressive carbon build-up can locally alter the wetting and accessibility of the catalyst layer, thereby perturbing the degradation mechanisms under investigation. This represents a serious potential artefact that must be carefully recognised and mitigated.

In the case of platinum-based electrocatalysts for PEM FCs, such contamination can have significant electrochemical consequences. A nanometer-thin carbonaceous overlayer deposited during prior SEM imaging may partially or fully encapsulate individual Pt nanoparticles. This encapsulation serves as a physical barrier, impeding electrolyte penetration and reactant access during subsequent electrochemical testing. Consequently, affected particles may appear artificially stable during ASTs, not due to intrinsic durability, but because of beam-induced passivation. This effect can lead to overestimation of catalyst stability and misinterpretation of degradation pathways.

An illustrative case, shown in Figure 6, was observed during an IL-SEM investigation of a GDE subjected to a severe degradation protocol designed to induce Pt dissolution (Protocol 2). The purpose of using this deliberately severe protocol was not to quantify Pt dissolution, but to create sufficiently strong electrochemical contrast to reveal the artefact caused by prior beam exposure: non-exposed regions undergo pronounced Pt depletion, whereas beam-exposed, carbon-contaminated regions may retain Pt and thus appear falsely stable. Under these conditions, most Pt nanoparticles were dissolved or exhibited pronounced morphological changes, consistent with the expected behaviour under highly aggressive electrochemical cycling. However, a central region retained a small cluster of Pt particles that remained entirely intact. This location had been exposed to prolonged high-magnification SEM imaging during an earlier session, plausibly resulting in localised formation of a carbonaceous overlayer due to electron-beam-induced hydrocarbon cracking. Such contamination can physically shield catalyst particles from electrochemical attack, producing a misleading appearance of stability and, in this case, a “false positive” in the degradation assessment.

https://doi.org/10.1021/acscatal.6c01369
ACS Catal. 2026, 16, 11207−11218

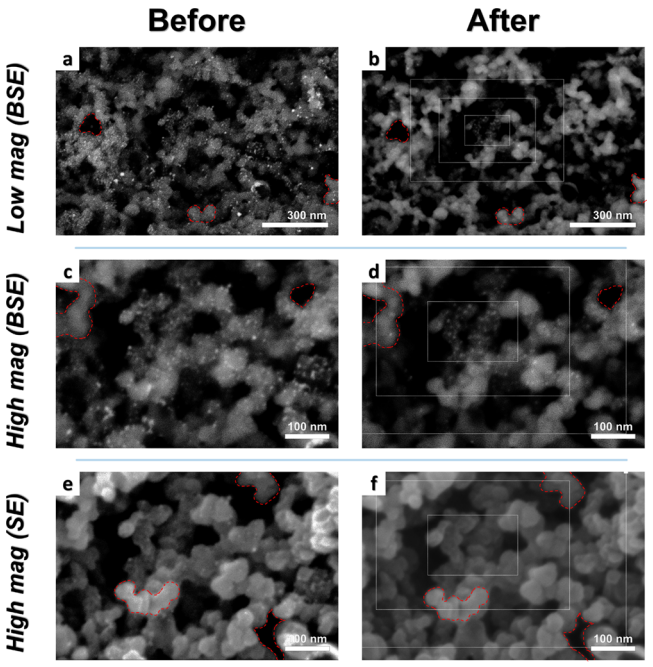

Figure 6. IL-SEM images of a PEM fuel cell catalyst layer before and after a severe Pt dissolution protocol (Protocol 2), highlighting localized resistance to beam-induced carbon contamination. (a, b) Low-magnification and (c, d) higher-magnification images acquired using backscattered electron (BSE) detection; (e, f) corresponding secondary electron (SE) images. Panels on the right (b, d, f) were acquired after repeated imaging of the regions indicated by rectangular frames, which mark areas subjected to increased cumulative electron-beam exposure. Red dashed contours mark identical fields of view to aid direct spatial correlation.

These observations highlight the importance of careful beam management during SEM-based PSD analysis and IL-SEM studies when results are correlated with electrochemical durability. Minimising dwell times, ensuring optimal vacuum conditions before starting an SEM session, avoiding repeated imaging of identical locations prior to electrochemical testing, choosing an oil-free vacuum system, and, equally important if not more so, performing routine chamber or specimen plasma cleaning can significantly reduce the risk of such artefacts. This example is presented as a cautionary note, underscoring the need to account for potential beam-induced artefacts when coupling SEM-based PSD with IL-SEM in electrochemistry studies, so that observed changes can be confidently attributed to genuine catalyst behaviour rather than imaging-induced effects.

Influence of the Membrane on Durability Studies in Half-Cell Systems

Having established the SEM-based PSD method and necessary precautions, we next applied IL-SEM to investigate how the presence of a proton-exchange membrane influences catalyst degradation during AST. We conducted identical AST (Protocol 1) on two sets of nominally identical GDE samples: one set without a membrane (catalyst layer directly immersed in liquid electrolyte) and one set with a thin PFSA membrane hot-pressed onto the catalyst layer (mimicking an MEA-like environment). By comparing these two scenarios, we can isolate the effect of the membrane on nanoparticle stability.

In the absence of a membrane (electrolyte-soaked catalyst; Figure 7a–c), most small Pt nanoparticles disappear, and the surface becomes dominated by large agglomerates. In contrast, the membrane-containing sample (Figure 7d–f) retains a substantial fraction of fine particles, with markedly fewer large clusters. Quantitatively, the membrane-free GDE exhibits a shift in median particle diameter from 4.0 nm (IQR: 3.3–4.8 nm) to 5.8 nm (IQR: 4.5–7.1 nm) after AST. In the presence of a membrane, the median increases only to 4.7 nm (IQR: 3.9–5.8 nm). These findings demonstrate that flooding of the catalyst layer with liquid acid substantially accelerates particle growth (Figure 7b,e). This interpretation is further supported by CO-stripping measurements before and after AST. The membrane-free GDE shows a substantially larger change in the CO-electrooxidation response than the GDE-PEM, including pronounced peak broadening and the appearance of a low-potential shoulder/prepeak, whereas the GDE-PEM changes less strongly. This trend is consistent with the stronger particle coarsening observed by IL-SEM in the membrane-free configuration.[41] Quantitatively, the membrane-free GDE exhibits an ECSA loss of approximately 32% and an estimated geometrical surface-area loss of approximately 31%, while the GDE-PEM shows smaller losses of approximately 16.5 and 15%, respectively. The corresponding voltammograms are provided in the Supporting Information.

This stark difference has a clear physical origin. In the absence of a membrane, the catalyst layer is directly exposed to concentrated liquid electrolyte, which promotes Pt dissolution. Dissolved Pt species can diffuse through the liquid phase and redeposit onto larger particles, facilitating pronounced coarsening (Ostwald ripening).[8,42,43] Under such conditions, proton availability is spatially unrestricted and transport is no longer dominated by the ionomer network.[44−46] Together, these effects indicate that degradation phenomena observed under membrane-free, electrolyte-flooded conditions may not fully represent catalyst-layer behaviour in operating PEM fuel cells. We note that the present analysis is intentionally focused on the morphological evolution and PSD changes of PtCo/C catalyst layers under different GDE configurations. Although alloy-specific compositional changes may occur during AST in PtCo/C systems, these were not directly assessed here; accordingly, the discussion is limited to the structural degradation behaviour resolved by IL-SEM/PSD analysis.

As a result, membrane-free configurations may not accurately reproduce the physicochemical conditions of PEM fuel-cell catalyst layers and can overestimate degradation severity.[42] In contrast, when a membrane is present, proton transport is confined to the ionomer-membrane interface and the catalyst layer is not in direct contact with bulk liquid acid.[45] The absence of a continuous liquid phase restricts long-range Pt transport, resulting in more localised and representative degradation behaviour.[44] In this regime, the membrane acts as a protective barrier that reduces the severity of degradation processes: membrane-free tests include a strong chemical dissolution component, whereas membrane-protected tests predominantly reflect electrochemically driven degradation.[8]

The pronounced coarsening observed in membrane-free GDEs is therefore not an inherent property of the catalyst, but a consequence of extended Pt migration ranges permitted by electrolyte flooding. In contrast, laminated GDEs restrict vertical transport and produce PSDs that more closely resemble degradation behaviour in operating MEAs.

https://doi.org/10.1021/acscatal.6c01369
ACS Catal. 2026, 16, 11207−11218

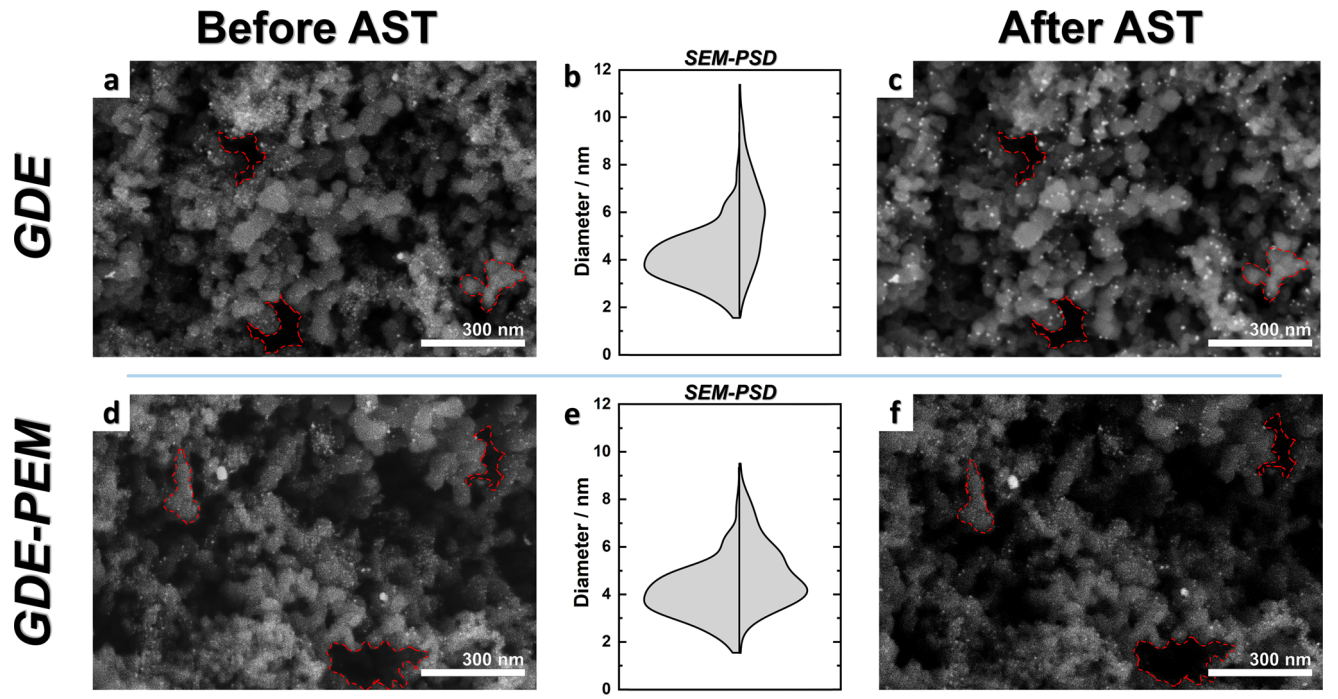

Figure 7. Effect of membrane presence on GDE degradation under AST. IL-SEM images of GDEs without membrane (a, c) and with membrane (GDE-PEM; d, f), before (a, d) and after (c, f) AST. The membrane-free GDE shows marked particle growth after AST, while the membrane-protected GDE preserves a more uniform dispersion (red dashed outlines indicate agglomerates). (b, e) SEM-derived particle size distributions (violin plots): left half before AST, right half after AST. Significant size broadening occurs without membrane, whereas membrane protection limits particle growth. Red dashed contours mark identical fields of view to aid direct spatial correlation.

To further confirm the role of the acidic environment in driving coarsening, we performed additional ASTs (Protocol 3) in which we varied the electrolyte concentration in the no-membrane configuration (Figure 8). We compared catalyst degradation in GDEs (without membrane) using 0.1 M, 0.5 M, and 2 M $HClO_4$, and also tested GDEs with a membrane under the same conditions. In the bare GDEs, higher acid concentration led to more severe particle coarsening, whereas dilution to 0.1 M significantly reduced the growth, though some ripening still occurred. This trend is consistent with thermodynamic expectations from Pt Pourbaix diagrams, which predict enhanced Pt dissolution kinetics at very low pH, particularly below pH 1.[46] In contrast, all the membrane-protected GDEs showed similarly restrained degradation regardless of acid concentration. This comparison confirms that it is the presence of aggressive pH in liquid acid and relatively fast diffusion of dissolved Pt ions that exaggerates the ripening,[47] and that the membrane's removal of that liquid exposure yields the more moderate, realistic degradation behaviour. Although further electrolyte dilution may in principle promote convergence between membrane-free and membrane-protected GDEs, the corresponding increase in HFR and transport limitations observed at lower acidities (see Supporting Information) indicates that this regime is not experimentally meaningful for the operating conditions considered here.

In essence, a membrane-free GDE half-cell closely resembles a floating-electrode-type configuration, in which the catalyst layer is fully flooded with electrolyte.[11] Under such conditions, oxygen transport limitations are largely alleviated (in contrast to typical RDE measurements), provided the catalyst layer is sufficiently thin, leading to unusually aggressive electrochemical environments.[48−50] Our results indicate that such floating-electrode or fully flooded half-cell tests can substantially overestimate catalyst degradation when 3D Ostwald ripening is one of the operative mechanisms. The harsh chemical environment (e.g., low pH or presence of chlorides) promotes exaggerated dissolution,[21] long-range diffusion of dissolved species, and their preferential redeposition on the most exposed regions of the catalyst layer, leading to coarsening levels that would not occur in a real fuel cell. By using IL-SEM on GDEs with a membrane, we see that much of the apparent degradation observed in the flooded case does not occur under more realistic conditions. This prevents misinterpretation: had we only examined the no-membrane data, we might have concluded that the catalyst was extremely unstable, whereas the membrane-protected data reveal far more moderate degradation. IL-SEM combined with SEM-based PSD analysis thus enables us to distinguish degradation arising from the test configuration from degradation observed under more realistic conditions.[14]

The observed mitigation of coarsening in membrane-laminated GDEs is not merely a geometric transport effect but reflects a shift in the local dissolution-redeposition equilibrium. In flooded electrodes, rapid diffusion of dissolved Pt species into the bulk electrolyte lowers their local concentration at the catalyst surface, reducing the probability of immediate redeposition and effectively favouring net dissolution. In contrast, membrane-imposed transport constraints increase the residence time of dissolved species within the catalyst layer, thereby enhancing local supersaturation and increasing the likelihood of redeposition onto neighbouring particles. As a result, the thermodynamic driving force for Ostwald ripening remains operative, but its spatial extent and kinetic expression are

https://doi.org/10.1021/acscatal.6c01369
ACS Catal. 2026, 16, 11207−11218

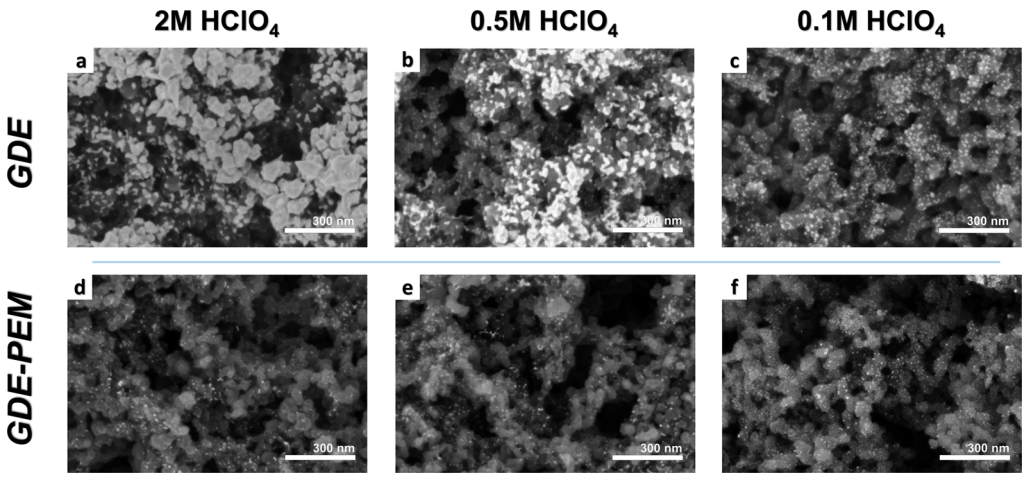

Figure 8. Influence of acid concentration on GDE degradation under severe AST (Protocol 3). (a–c) SEM images of GDEs without membrane after AST in 2 M, 0.5 M, and 0.1 M $HClO_4$, respectively. Strong particle coarsening is evident at high acid concentrations, gradually decreasing with dilution. (d–f) Corresponding GDEs with membrane protection show significantly reduced ripening across all conditions, maintaining a finer and more uniform particle distribution.

fundamentally altered. Flooded configurations therefore exaggerate long-range ripening by decoupling dissolution from redeposition, whereas membrane-constrained systems preserve the coupled dynamics characteristic of operating PEMFC catalyst layers.

It should be noted that introducing the membrane, while essential for realistic results, also introduces the typical complexities of an MEA environment. For example, the catalyst layer must have a well-developed ionomer network and be well-bonded to the membrane to ensure effective proton conduction; similarly, proper humidification of the membrane and ionomer is necessary before high-current operation. These practical considerations become important when moving towards more realistic tests.

Ehelebe et al.[8] previously examined membrane effects using ICP-MS to monitor dissolved Pt in the electrolyte. While their conclusions are directionally consistent with ours, electrolyte-phase Pt signals alone cannot distinguish between genuine mitigation of catalyst-layer ripening and altered Pt transport or temporary retention within the membrane. Our ex-situ microscopic analysis directly quantifies PSD evolution within the CL, complementing electrolyte analytics and strengthening the mechanistic understanding. As a further step toward still more realistic catalyst durability assessment, the present IL-SEM-PSD methodology could in principle be extended to full MEAs, consistent with recent demonstrations of identical-location electron microscopy in operating PEMFC environments.[15,51]

Overall, this case study demonstrates that automated IL-SEM combined with PSD analysis provides a quantitative and realistic view of catalyst degradation in GDE systems. By enabling direct observation of nanoparticle evolution under conditions that closely mimic true PEMFC operation, this approach establishes a robust framework for assessing catalyst durability and for bridging microscopic characterisation with electrochemical performance. Beyond this specific application, integrating high-resolution SEM imaging with identical-location tracking offers deep, quantitative insight into catalyst nanostructure and its evolution during operation. By leveraging IL-SEM, catalyst ageing can be evaluated in-situ within realistic, micrometer-thick porous catalyst architectures, thereby guiding the design of more durable catalysts and more representative testing protocols. Collectively, these techniques open new avenues for catalyst diagnostics and durability studies by uniting electron microscopy and electrochemical testing into a single, comprehensive analytical framework.

4. CONCLUSIONS

This study demonstrates that the presence of a proton-exchange membrane significantly affects degradation behaviour in PtCo/C catalyst layers during accelerated stress testing in GDE half-cell configurations. Membrane-free electrodes allow extensive redistribution of dissolved Pt species across the catalyst layer, promoting pronounced three-dimensional coarsening that spans across the catalyst-layer thickness. We hypothesise that this behaviour results not only from enhanced Pt ion transport but also from a shift in the local dissolution-redeposition equilibrium: rapid dilution of dissolved Pt species reduces their local concentration, thereby lowering the likelihood of immediate redeposition and effectively favouring net dissolution. In contrast, laminated GDEs introduce additional mass-transport limitations that confine dissolved Pt species spatially, increasing the probability of local redeposition and thus moderating both net dissolution and overall coarsening. In practice, the observed degradation likely reflects a dynamic interplay between transport constraints and thermodynamically governed dissolution-redeposition processes.

These findings indicate that membrane-free half-cells can substantially overestimate catalyst degradation and may provide an incomplete representation of electrocatalyst stability under realistic PEM fuel cell operating conditions.

Although demonstrated here for PtCo/C catalysts, the mechanistic principles identified are not material-specific. Any electrocatalyst system in which degradation proceeds via dissolution-migration-redeposition dynamics will be intrinsically sensitive to transport constraints imposed by membrane or ionomer architecture. The implications therefore extend

https://doi.org/10.1021/acscatal.6c01369
ACS Catal. 2026, 16, 11207–11218

beyond the specific catalyst studied and suggest a broader methodological consequence: half-cell durability tests that omit membrane confinement may systematically overestimate catalyst instability whenever long-range migration contributes to degradation. Incorporating realistic transport constraints is thus essential for meaningful and transferable catalyst benchmarking.

To investigate degradation under more representative structural conditions, we developed and validated an IL-SEM-based methodology for quantifying nanoparticle size distributions directly within intact, micrometer-thick porous catalyst layers. Comparison with IL-TEM confirms quantitative agreement for surface-accessible particles, while automated segmentation enables reproducible, high-throughput analysis across statistically significant datasets. By preserving the native electrode architecture, IL-SEM provides access to degradation phenomena that remain inaccessible in thin-film model systems.

The integration of membrane-aware GDE testing with IL-SEM-based particle size distribution analysis establishes a realistic and scalable framework for evaluating electrocatalyst durability. This combined approach enables correlation of nanoscale morphological evolution with electrochemical performance and provides a robust basis for assessing catalyst stability under PEM fuel cell-relevant conditions.

■ ASSOCIATED CONTENT

Supporting Information

The Supporting Information is available free of charge at https://pubs.acs.org/doi/10.1021/acscatal.6c01369.

Additional materials and methods; sample preparation and electrochemical operation; GDE and modified floating electrode half-cell setups; additional SEM and IL-SEM methodological details; automated image-segmentation pipeline; additional IL-SEM/TEM validation and segmentation calibration; expanded results for MFE versus GDE, carbon contamination, membrane influence, and acid-concentration effects; CO-stripping/ECSA and HFR analyses; supplementary discussion; references (DOCX)

■ AUTHOR INFORMATION

Corresponding Authors

Mitja Kostelec – *Department of Materials Chemistry, National Institute of Chemistry, Hajdrihova ulica 19, Ljubljana 1001, Slovenia; University of Nova Gorica, Vipavska 13, Nova Gorica SI-5000, Slovenia;* orcid.org/0009-0004-9884-3221; Email: mitja.kostelec@ki.si

Nejc Hodnik – *Department of Materials Chemistry, National Institute of Chemistry, Hajdrihova ulica 19, Ljubljana 1001, Slovenia; University of Nova Gorica, Vipavska 13, Nova Gorica SI-5000, Slovenia; Institute of Metals and Technology, Lepi pot 11, Ljubljana 1000, Slovenia;* orcid.org/0000-0002-7113-9769; Email: nejc.hodnik@ki.si

Authors

Goran Dražić – *Department of Materials Chemistry, National Institute of Chemistry, Hajdrihova ulica 19, Ljubljana 1001, Slovenia;* orcid.org/0000-0001-7809-8050

Ana Rebeka Kamšek – *Department of Materials Chemistry, National Institute of Chemistry, Hajdrihova ulica 19, Ljubljana 1001, Slovenia; Faculty of Chemistry and Chemical Technology, University of Ljubljana, Večna pot 113, Ljubljana 1000, Slovenia; Institute of Metals and Technology, Lepi pot 11, Ljubljana 1000, Slovenia;* orcid.org/0009-0008-6247-3256

Jan Vidergar – *Department of Materials Chemistry, National Institute of Chemistry, Hajdrihova ulica 19, Ljubljana 1001, Slovenia; Faculty of Chemistry and Chemical Technology, University of Ljubljana, Večna pot 113, Ljubljana 1000, Slovenia*

Gregor Kapun – *Department of Materials Chemistry, National Institute of Chemistry, Hajdrihova ulica 19, Ljubljana 1001, Slovenia; Faculty of Chemistry and Chemical Technology, University of Ljubljana, Večna pot 113, Ljubljana 1000, Slovenia;* orcid.org/0000-0003-0007-4678

Complete contact information is available at: https://pubs.acs.org/doi/10.1021/acscatal.6c01369

Author Contributions

M.K.: Conceptualization, methodology, investigation (SEM, GDE), data curation, formal analysis, validation, visualisation, project administration, writing—original draft, writing— review and editing. G.D.: Investigation (TEM), writing—review and editing (TEM). A.R.K.: Methodology (automated image segmentation), writing—review and editing (automated image segmentation). J.V.: Methodology (automated image segmentation). G.K.: Validation, writing—review and editing (SEM). N.H.: Resources, supervision, funding acquisition, writing—review and editing.

Notes

The authors declare no competing financial interest.

■ ACKNOWLEDGMENTS

The authors acknowledge the Slovenian Research Agency (ARRS) for support through programs P2-0421, P2-0393, and I0−0003 and projects RZK-26007, GC-0001, GC-0003, GC-0004, N2-0248, N2-0257, J7-4637, and J2-60043. A.R.K. acknowledges support from the Janko Jamnik Doctoral Scholarship. M.K. acknowledges funding from EKPO Fuel Cell Technologies GmbH. The authors also thank North Atlantic Treaty Organization Science for Peace and Security (NATO SPS) program (grant G6230). The authors acknowledge partial support from the Republic of Slovenia, the Ministry of Higher Education, Science and Innovation, and the European Union—NextGenerationEU in the framework of the project HyBReED, part of the Slovenian Recovery and Resilience Plan. Views and opinions expressed are however those of the authors only and do not necessarily reflect those of the Republic of Slovenia, the Ministry of Higher Education, the European Union, or the European Commission. Neither the Republic of Slovenia, the Ministry of Higher Education, Science and Innovation, the European Union nor the European Commission can be held responsible for them.

■ REFERENCES

(1) Girod, R.; Lazaridis, T.; Gasteiger, H. A.; Tileli, V. Three-Dimensional Nanoimaging of Fuel Cell Catalyst Layers. *Nat. Catal.* **2023**, *6* (5), 383–391.

(2) Kostelec, M.; Gatalo, M.; Hodnik, N. Fundamental and Practical Aspects of Break-In/Conditioning of Proton Exchange Membrane Fuel Cells. *Chem. Rec.* **2024**, *24* (10), No. e202400114.

(3) Suter, T. A. M.; Smith, K.; Hack, J.; Rasha, L.; Rana, Z.; Angel, G. M. A.; Shearing, P. R.; Miller, T. S.; Brett, D. J. L. Engineering Catalyst Layers for Next-Generation Polymer Electrolyte Fuel Cells: A Review of Design, Materials, and Methods. *Adv. Energy Mater.* **2021**, *11* (37), No. 2101025.
(4) Bijelić, L.; Ruiz-Zepeda, F.; Hodnik, N. The Role of High-Resolution Transmission Electron Microscopy and Aberration Corrected Scanning Transmission Electron Microscopy in Unraveling the Structure−Property Relationships of Pt-Based Fuel Cells Electrocatalysts. *Inorg. Chem. Front.* **2024**, *11* (2), 323–341.
(5) Arenz, M.; Zana, A. Fuel Cell Catalyst Degradation: Identical Location Electron Microscopy and Related Methods. *Nano Energy* **2016**, *29*, 299–313.
(6) Yano, H.; Watanabe, M.; Iiyama, A.; Uchida, H. Particle-Size Effect of Pt Cathode Catalysts on Durability in Fuel Cells. *Nano Energy* **2016**, *29*, 323–333.
(7) U.S. DRIVE Fuel Cell Technical Team. *Fuel Cell Technical Team Roadmap*; U.S. Department of Energy: Washington, DC, **2017**. https://www.energy.gov/eere/vehicles/articles/us-drive-fuel-cell-technical-team-roadmap.
(8) Ehelebe, K.; Knöppel, J.; Bierling, M.; Mayerhöfer, B.; Böhm, T.; Kulyk, N.; Thiele, S.; Mayrhofer, K. J. J.; Cherevko, S. Platinum Dissolution in Realistic Fuel Cell Catalyst Layers *Angew. Chem.* **2021** *133* (16) 8964–8970.
(9) Cherevko, S.; Keeley, G. P.; Geiger, S.; Zeradjanin, A. R.; Hodnik, N.; Kulyk, N.; Mayrhofer, K. J. J. Dissolution of Platinum in the Operational Range of Fuel Cells. *ChemElectroChem* **2015**, *2* (10), 1471–1478.
(10) Ehelebe, K.; Escalera-López, D.; Cherevko, S. Limitations of Aqueous Model Systems in the Stability Assessment of Electrocatalysts for Oxygen Reactions in Fuel Cell and Electrolyzers. *Curr. Opin. Electrochem.* **2021**, *29*, No. 100832.
(11) Topalov, A. A.; Cherevko, S.; Zeradjanin, A. R.; Meier, J. C.; Katsounaros, I.; Mayrhofer, K. J. J. Towards a Comprehensive Understanding of Platinum Dissolution in Acidic Media. *Chem. Sci.* **2014**, *5* (2), 631–638.
(12) Hodnik, N.; Zorko, M.; Jozinović, B.; Bele, M.; Dražič, G.; Hočevar, S.; Gaberšček, M. Severe Accelerated Degradation of PEMFC Platinum Catalyst: A Thin Film IL-SEM Study. *Electrochem. Commun.* **2013**, *30*, 75–78.
(13) Yu, H.; Zachman, M. J.; Li, C.; Hu, L.; Kariuki, N. N.; Mukundan, R.; Xie, J.; Neyerlin, K. C.; Myers, D. J.; Cullen, D. A. Recreating Fuel Cell Catalyst Degradation in Aqueous Environments for Identical-Location Scanning Transmission Electron Microscopy Studies. *ACS Appl. Mater. Interfaces* **2022**, *14* (18), 20418–20429.
(14) Hodnik, N.; Cherevko, S. Spot the Difference at the Nanoscale: Identical Location Electron Microscopy in Electrocatalysis. *Curr. Opin. Electrochem.* **2019**, *15*, 73–82.
(15) Shokhen, V.; Strandberg, L.; Skoglundh, M.; Wickman, B. Fuel Cell Electrode Degradation Followed by Identical Location Transmission Electron Microscopy. *J. Mater. Chem. A* **2023**, *11* (39), 21029–21035.
(16) Hrnjić, A.; Ruiz-Zepeda, F.; Gaberšček, M.; Bele, M.; Suhadolnik, L.; Hodnik, N.; Jovanovič, P. Modified Floating Electrode Apparatus for Advanced Characterization of Oxygen Reduction Reaction Electrocatalysts. *J. Electrochem. Soc.* **2020**, *167* (16) No. 166501.
(17) Hettler, S.; Dries, M.; Hermann, P.; Obermair, M.; Gerthsen, D.; Malac, M. Carbon Contamination in Scanning Transmission Electron Microscopy and Its Impact on Phase-Plate Applications. *Micron* **2017**, *96*, 38–47.
(18) Schindelin, J.; Arganda-Carreras, I.; Frise, E.; Kaynig, V.; Longair, M.; Pietzsch, T.; Preibisch, S.; Rueden, C.; Saalfeld, S.; Schmid, B.; Tinevez, J.-Y.; White, D. J.; Hartenstein, V.; Eliceiri, K.; Tomancak, P.; Cardona, A. Fiji: An Open-Source Platform for Biological-Image Analysis. *Nat. Methods* **2012**, *9* (7), 676–682.
(19) Aviles, K. M.; Lear, B. J. Practical Guide to Automated TEM Image Analysis for Increased Accuracy and Precision in the Measurement of Particle Size and Morphology. *ACS Nanosci. Au* **2025**, *5* (3), 117–127.
(20) Yu, H.; Zachman, M. J.; Reeves, K. S.; Park, J. H.; Kariuki, N. N.; Hu, L.; Mukundan, R.; Neyerlin, K. C.; Myers, D. J.; Cullen, D. A. Tracking Nanoparticle Degradation across Fuel Cell Electrodes by Automated Analytical Electron Microscopy. *ACS Nano* **2022**, *16* (8), 12083–12094.
(21) Zorko, M.; Jozinović, B.; Bele, M.; Hodnik, N.; Gaberšček, M. SEM Method for Direct Visual Tracking of Nanoscale Morphological Changes of Platinum Based Electrocatalysts on Fixed Locations upon Electrochemical or Thermal Treatments. *Ultramicroscopy* **2014**, *140*, 44–50.
(22) Thiele, P.; Yang, Y.; Dirkes, S.; Wick, M.; Pischinger, S. Realistic Accelerated Stress Tests for PEM Fuel Cells: Test Procedure Development Based on Standardized Automotive Driving Cycles. *Int. J. Hydrogen Energy* **2024**, *52*, 1065–1080.
(23) Pahon, E.; Hissel, D.; Yousfi-Steiner, N. A Review of Accelerated Stress Tests Dedicated to Proton Exchange Membrane Fuel Cells − Part I: Fuel Cell Component Level. *J. Power Sources* **2022**, *546* (April), No. 231895.
(24) Heizmann, P. A.; Nguyen, H.; Holst, M.von; Fischbach, A.; Kostelec, M.; Gonzalez Lopez, F. J.; Bele, M.; Pavko, L.; Đukić, T.; Šala, M.; Ruiz-Zepeda, F.; Klose, C.; Gatalo, M.; Hodnik, N.; Vierrath, S.; Breitwieser, M. Alternative and Facile Production Pathway towards Obtaining High Surface Area PtCo/C Intermetallic Catalysts for Improved PEM Fuel Cell Performance. *RSC Adv.* **2023**, *13* (7), 4601–4611.
(25) Fuel Cell Store. *Sigracet 39 BB* **2026** https://www.fuelcellstore.com/sigracet-39-bb-carbon-paper-gdl.
(26) Fuel Cell Store *PFSA D15-R ePTFE Reinforced Proton Exchange Membrane*. **2026**. https://www.fuelcellstore.com/pfsa-d15r-eptfe-reinforced-proton-exchange-membrane-87010032.
(27) Wandrol, P.; Vesseur, E. J R; Vasina, R.; Ilitchev, A.*Advanced SEM Imaging with the Trinity Detection System* **2019**.
(28) Thermo Fisher Scientific, *Benefits of Low-KeV Imaging on Beam-Sensitive Materials: Apreo 2 SEM Imaging of Calcium Carbonate (CaCO3) Particles*; **2022**. https://documents.thermofisher.com/TFS-Assets/MSD/Application-Notes/benefits-low-kev-imaging-beam-sensitive-materials-en-an0186.pdf.
(29) Thermo Fisher Scientific *Apreo 2 SEM: Unmatched Versatility Powered by ChemiSEM Technology* **2024**. https://documents.thermofisher.com/TFS Assets/MSD/Datasheets/Apreo-SEM-Datasheet.pdf.
(30) Tomc, B.; Bele, M.; Kamšek, A. R.; Martins, M.; Marsel, A.; Hotko, M.; Popović, S.; Kapun, G.; Donik, Č.; Kostelec, M.; Godec, M.; Hodnik, N.; Suhadolnik, L. Workflow and Practical Guidance for Identical Location Scanning Electron Microscopy: Reliable Tracking of Localized Transformations. *Small Methods* **2025**, 1–169.
(31) GDE *Gas Diffusion Electrode Cell*. **2026** www.gde-cell.com.
(32) Matsumoto, M.; Miyazaki, T.; Imai, H. Oxygen-Enhanced Dissolution of Platinum in Acidic Electrochemical Environments. *J. Phys. Chem. C* **2011**, *115* (22), 11163–11169.
(33) Bae, J. H.; Brocenschi, R. F.; Kisslinger, K.; Xin, H. L.; Mirkin, M. V. Dissolution of Pt during Oxygen Reduction Reaction Produces Pt Nanoparticles. *Anal. Chem.* **2017**, *89* (23), 12618–12621.
(34) Eaton, P.; Quaresma, P.; Soares, C.; Neves, C.; Almeida, M. P.de; Pereira, E.; West, P. A Direct Comparison of Experimental Methods to Measure Dimensions of Synthetic Nanoparticles. *Ultramicroscopy* **2017**, *182*, 179–190.
(35) Chen, S.; Gasteiger, H. A.; Hayakawa, K.; Tada, T.; Shao-Horn, Y. Platinum-Alloy Cathode Catalyst Degradation in Proton Exchange Membrane Fuel Cells: Nanometer-Scale Compositional and Morphological Changes. *J. Electrochem. Soc.* **2010**, *157* (1), No. A82.
(36) Koderman Podboršek, G.; Suhadolnik, L.; Lončar, A.; Bele, M.; Hrnjić, A.; Marinko, Ž.; Kovač, J.; Kokalj, A.; Gašparič, L.; Surca, A. K.; Kamšek, A. R.; Dražić, G.; Gaberšček, M.; Hodnik, N.; Jovanovič, P. Iridium Stabilizes Ceramic Titanium Oxynitride Support for Oxygen Evolution Reaction. *ACS Catal.* **2022**, *12* (24), 15135–15145.

https://doi.org/10.1021/acscatal.6c01369
ACS Catal. 2026, 16, 11207−11218

(37) Kamšek, A. R. *Particle-Segmentation*; GitHub.**2026** https://github.com/kamsekar/Particle-segmentation.
(38) Egerton, R. F.; Li, P.; Malac, M. Radiation Damage in the TEM and SEM. *Micron* **2004**, *35* (6), 399–409.
(39) Egerton, R. F. Radiation Damage to Organic and Inorganic Specimens in the TEM. *Micron* **2019**, *119*, 72–87.
(40) Hugenschmidt, M.; Adrion, K.; Marx, A.; Müller, E.; Gerthsen, D. Electron-Beam-Induced Carbon Contamination in STEM-in-SEM: Quantification and Mitigation. *Microsc. Microanal.* **2023**, *29* (1), 219–234.
(41) Maillard, F.; Schreier, S.; Hanzlik, M.; Savinova, E. R.; Weinkauf, S.; Stimming, U. Influence of Particle Agglomeration on the Catalytic Activity of Carbon-Supported Pt Nanoparticles in CO Monolayer Oxidation. *Phys. Chem. Chem. Phys.* **2005**, *7* (2), 385–393.
(42) Borup, R.; Meyers, J.; Pivovar, B.; Kim, Y. S.; Mukundan, R.; Garland, N.; Myers, D.; Wilson, M.; Garzon, F.; Wood, D.; Zelenay, P.; More, K.; Stroh, K.; Zawodzinski, T.; Boncella, J.; McGrath, J. E.; Inaba, M.; Miyatake, K.; Hori, M.; Ota, K.; Ogumi, Z.; Miyata, S.; Nishikata, A.; Siroma, Z.; Uchimoto, Y.; Yasuda, K.; Kimijima, K.; Iwashita, N. Scientific Aspects of Polymer Electrolyte Fuel Cell Durability and Degradation. *Chem. Rev.* **2007**, *107* (10), 3904–3951.
(43) Mayrhofer, K. J. J.; Hartl, K.; Juhart, V.; Arenz, M. Degradation of Carbon-Supported Pt Bimetallic Nanoparticles by Surface Segregation. *J. Am. Chem. Soc.* **2009**, *131* (45), 16348–16349.
(44) Kongkanand, A.; Mathias, M. F. The Priority and Challenge of High-Power Performance of Low-Platinum Proton-Exchange Membrane Fuel Cells. *J. Phys. Chem. Lett.* **2016**, *7* (7), 1127–1137.
(45) Weber, A. Z.; Newman, J. Modeling Transport in Polymer-Electrolyte Fuel Cells. *Chem. Rev.* **2004**, *104* (10), 4679–4726.
(46) Cherevko, S.; Kulyk, N.; Mayrhofer, K. J. J. Durability of Platinum-Based Fuel Cell Electrocatalysts: Dissolution of Bulk and Nanoscale Platinum. *Nano Energy* **2016**, *29*, 275–298.
(47) Imhof, T.; Della Bella, R. K. F.; Stühmeier, B. M.; Gasteiger, H. A.; Ledendecker, M. Towards a Realistic Prediction of Catalyst Durability from Liquid Half-Cell Tests. *Phys. Chem. Chem. Phys.* **2023**, *25* (30), 20533–20545.
(48) Schmitt, N.; Schmidt, M.; Mueller, J. E.; Schmidt, L.; Trabold, M.; Jeschonek, K.; Etzold, B. J. M. Which Insights Can Gas Diffusion Electrode Half-Cell Experiments Give into Activity Trends and Transport Phenomena of Membrane Electrode Assemblies? *Energy Adv.* **2023**, *2* (6), 854–863.
(49) Martens, S.; Asen, L.; Ercolano, G.; Dionigi, F.; Zalitis, C.; Hawkins, A.; Martinez Bonastre, A.; Seidl, L.; Knoll, A. C.; Sharman, J.; Strasser, P.; Jones, D.; Schneider, O. A Comparison of Rotating Disc Electrode, Floating Electrode Technique and Membrane Electrode Assembly Measurements for Catalyst Testing. *J. Power Sources* **2018**, *392*, 274–284.
(50) Ehelebe, K.; Seeberger, D.; Paul, M. T. Y.; Thiele, S.; Mayrhofer, K. J. J.; Cherevko, S. Evaluating Electrocatalysts at Relevant Currents in a Half-Cell: The Impact of Pt Loading on Oxygen Reduction Reaction. *J. Electrochem. Soc.* **2019**, *166* (16), F1259–F1268.
(51) Strandberg, L.; Shokhen, V.; Skoglundh, M.; Wickman, B. Carbon Support Corrosion in PEMFCs Followed by Identical Location Electron Microscopy. *ACS Catal.* **2024**, *14* (11), 8494–8504.

https://doi.org/10.1021/acscatal.6c01369
ACS Catal. 2026, 16, 11207–11218